In situ X-Ray Powder Diffraction Investigation on the Development of Zeolite-Templated Carbons in FAU zeolite

Thibaud Aumond, Martin Esteves, Cristian Mocuta, Isabelle Batonneau-Gener, Julien Haines, Ricardo Faccio, Alexander Sachse

Chemistry—Methods

Research Article
doi.org/10.1002/cmtd.202400018

Chemistry Europe
European Chemical Societies Publishing

www.chemistrymethods.org

In situ X-Ray Powder Diffraction Investigation on the Development of Zeolite-Templated Carbons in FAU zeolite

Thibaud Aumond,[a] Martin Esteves,[b] Cristian Mocuta,[c] Isabelle Batonneau-Gener,[a] Julien Haines,[d] Ricardo Faccio,[b] and Alexander Sachse*[a]

A time resolved *in situ* X-ray powder diffraction study using synchrotron radiation allowed for describing the evolution of the zeolite **FAU** structure during the development of a zeolite-templated carbon (ZTC) in its porous voids. During the ZTC formation the intensity decrease of most zeolite reflections and the simultaneous rise in intensity of the 222 reflection (of null intensity in the pristine zeolite) was observed. Full pattern profile fitting by Rietveld refinement allowed for achieving a detailed description of the underlying chemistry, with coincident pore filling with carbon atoms in specific positions and framework distortion. Monitoring the intensity profiles of the 222 reflection allowed assessment of the energetics of the ZTC formation. Our results contribute to a better understanding of the phenomena involved on the atomic scale in ZTC synthesis.

Introduction

Zeolites are crucial components in numerous industrial catalyst formulations and are predominantly employed in hydrocarbon transformation processes.[1,2] The stability of these catalysts is significantly impacted by the formation of polyaromatic secondary reaction products, commonly known as coke,[3] which has led to extensive research efforts aimed at developing effective coke mitigation strategies.[4] However, there is also a domain where controlled coke formation is desirable, as in the case of Zeolite-Templated Carbons (ZTCs).

ZTCs exhibit unique textural properties, directly attributable to the formation of a carbon skeleton within the microporous voids of the sacrificial zeolite. The zeolite plays a dual role: its active sites catalyze the formation of a polyaromatic carbon network, while its micropore topology imposes steric constraints that limit the extension of the carbon skeleton.[5] Upon removal of the zeolite, the resulting ZTC retains a high micropore volume and electrical conductivity-properties that are highly advantageous for the design of advanced electrodes in energy conversion and storage devices.[6]

Despite the growing interest in ZTC materials, there remains a gap in understanding their formation, likely due to the challenges in characterizing the carbon materials after the zeolite template has been removed. These challenges are compounded by the still poorly understood modifications that occur within the carbon skeleton during template elimination.[7,8] In this context, studying the carbon/zeolite hybrid materials provides a valuable opportunity to gain insights into the chemical and structural evolution of ZTCs. For instance, *in situ* thermogravimetric analysis (TGA) of Na–Y zeolite during carbon/zeolite hybrid formation has revealed the existence of three distinct kinetic stages, which suggest the development of individual nanographene entities that condense during heat treatment.[9,10] Our group has recently identified the key steps in ZTC formation through a comprehensive *ex situ* kinetic study of carbon/zeolite hybrid formation, employing techniques such as gas physisorption, Raman spectroscopy, Continuous-Wave Electron Paramagnetic Resonance, Hyperfine Sublevel Correlation spectroscopy, and online Gas Chromatography.[7] This study revealed the rapid nucleation of small polyaromatic hydrocarbon species, which subsequently grow to fill the zeolite voids before condensing to form the carbon network. Furthermore, the characterization of carbon/zeolite hybrids has provided insights into the previously unclear impact of zeolite properties on the resulting ZTCs.[5]

X-ray powder diffraction (XRPD) is a powerful tool for characterizing zeolites from a structural perspective.[11] However, only a limited number of studies have reported the evolution of XRPD patterns in zeolites during the formation of hydrocarbon species within their porous voids. Modifications in the XRPD patterns of ZSM-5 zeolites during coking have been observed and attributed to lattice distortion,[12,13] with structural calculations revealing a phase transition to the orthorhombic form.[14,15] For **FAU**-type structures, only one study has discussed the XRPD patterns of H–Y zeolites during coking.[16] The authors observed no changes in the XRPD patterns at 200 °C but reported a slight expansion of the unit cell parameter by 0.01 nm for reactions conducted above 250 °C, suggesting that this might be related

[a] *Institut de Chimie des Milieux et Matériaux de Poitiers (IC2MP) – UMR 7285, CNRS, Université de Poitiers, Poitiers, France*
[b] *Centro NanoMat & Area Física, Departamento de Experimentacíon y Teoría de la Estructura de la Materia y sus Aplicaciones (DETEMA), Facultad de Química, Universidad de la República, Montevideo, Uruguay*
[c] *Synchrotron SOLEIL, Gif-sur-Yvette, France*
[d] *Institut Charles Gerhardt Montpellier, CNRS, Université de Montpellier, ENSCM, Montpellier, France*

***Correspondence:** Dr. Alexander Sachse, Institut de Chimie des Milieux et Matériaux de Poitiers (IC2MP) – UMR 7285, CNRS, Université de Poitiers, 4, rue Michel Brunet, 86073 Cedex 9 Poitiers, France.*
Email: alexander.sachse@univ-poitiers.fr

Supporting Information for this article is available on the WWW under https://doi.org/10.1002/cmtd.202400018

Research Article
doi.org/10.1002/cmtd.202400018
Chemistry Europe
European Chemical Societies Publishing

to the nature of the coke species forming at different temperatures. However, the XRPD patterns were not presented, and structural refinement was not conducted. Ryoo and colleagues have reported an electron-density map obtained through X-ray single-crystal diffraction of carbon/zeolite **FAU** hybrids, proposing nine possible positions for carbon atoms within the zeolite voids.[17]

In this study, we present a time-resolved *in situ* synchrotron XRPD investigation of ZTC formation using ethylene in H-USY (**FAU**) zeolite. The combination of experimental and theoretical analyses has enabled us to elucidate the structural modifications occurring during this process and to calculate its energetics.

Results and Discussion

In situ synchrotron XRPD patterns were recorded on the powder diffraction station of the DiffAbs beamline at SOLEIL synchrotron.[18] The **FAU** structured zeolite (protonic Y zeolite, Si/Al = 2.6) was filled in a quartz capillary and fixed with quartz wool. The capillary was then placed in the sample holder and introduced into an oven featuring two opposite apertures allowing for recording XRPD patterns in transmission mode (**Figure S1**). XRPD patterns were recorded with time intervals of 2 minutes using 17.919 keV (λ = 0.06919 nm) radiation. A blank experiment was performed, in which the zeolite was maintained at 680 °C under argon flow during 8 h (**Figure S2**). The position, intensity and FWHM of the zeolite reflections remained constant throughout the blank experiment, indicating the stability of the zeolite structural features at this temperature.

An experiment was then performed in which the gas composition was switched to 2.5 wt% ethylene in argon at 680 °C. After 20 min of the start of ethylene feeding a steady intensity decrease of the zeolite reflections was observed (Figure 1). Simultaneously, the evolution of a peak centered at 5.63° 2θ was recorded. Structural refinement allowed for ascribing the emerging peak to the 222 reflection of the **FAU** structure (**Figure S3**). It is interesting to note that this reflection is of null intensity in the pristine zeolite and features a linear growth until 140 min of ethylene feeding, reaching 60% of the maximal peak intensity. Thereafter, the intensity accretion is more progressive and a plateau is attained after approximately 400 min of ethylene feeding. It is interesting to note that the mass gain during carbon/zeolite hybrid formation was previously reported to follow a linear trend up to 60% of total carbon content.[7] This suggests that the intensity rise of the 222 reflection might be proportional to the amount of carbon forming within the zeolite pores.

The intensity increase of the 222 reflection in **FAU** zeolites was previously reported in a scarce number of publications. Sakamoto *et al.*[19] reported the development of the 222 reflection upon the formation of MoS_2 clusters in Na–Y zeolite. The authors surmised on a possible electron distribution with antisymmetric character with respect to the centers of the supercages upon cluster formation. It was further described that the La^{3+} exchange in Y zeolites previous to calcination

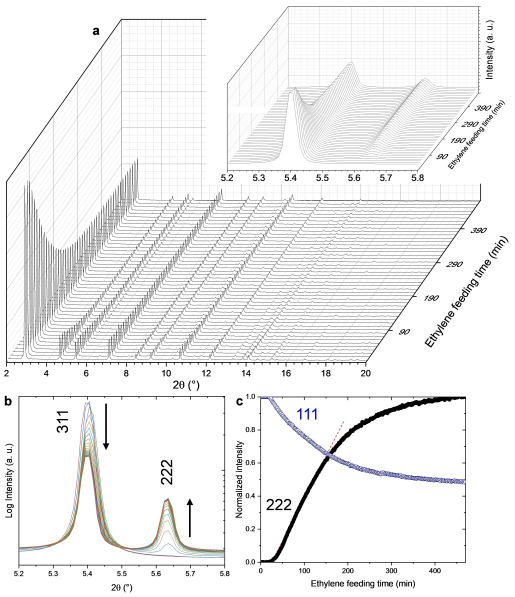

Figure 1. a) Time resolved *in situ* XRPD patterns (λ = 0.06919 nm) of H–Y zeolite during ZTC formation at 680 °C. The insert presents a magnification of the 5.2°–5.8° 2θ region. b) Evolution of XRPD patterns with logarithmic intensity scale in the 5.2°–5.8° 2θ region. c) Intensity evolution of the 111 (blue) and 222 (black) reflections.

strengthens the 222 reflection importantly.[20–22] It was speculated that an increase in electron density near the cation exchange position III would lead to the modifications in the XRD patterns.[23] The intensification of the 222 reflection in Na–Y zeolite was further evidenced upon benzene physisorption, suggesting that the hydrocarbon primarily adsorbs onto cations positioned at exchange site III within the supercages and in the 12-ring windows.[24–25]

It is hence reasonable to assess the possibility to study the evolution of the ZTC skeleton within the zeolite **FAU** voids by theoretically investigating the intensity evolution of the 222 reflection. It is worth mentioning that we observed intensity evolution of the 222 reflection in carbon/FAU hybrids for a wide range of Si/Al ratios and for different carbon precursors.[26]

The **FAU** framework is constructed by sodalite or β-cages linked through 4 of the 8 hexagonal faces to 6–6 secondary building units (double six-rings, D6R). This leads to the formation of larger voids (supercages), which feature a diameter of ca. 13 Å. Supercages are connected through four 12-ring windows of ca. 7.4 Å, allowing to generate the 3D microporous system (Scheme 1). Due to the narrow opening of 6-rings, the diffusion of ethylene, and hence carbon formation, is considered exclusively to occur in the micropore void system built by the arrangement of supercages.

A full pattern profile fitting using the Rietveld method was applied to the whole data set, considering the **FAU** structure with the space group $Fd\bar{3}m$, a lattice parameter a = 24.3097(8) Å and a Si/Al occupation fraction of 2.6 (Figure 2, Table 1). Based on the previously reported benzene adsorption experiments in **FAU** zeolite[24–25] refinement of the two Wyckoff

Research Article
doi.org/10.1002/cmtd.202400018

Chemistry Europe
European Chemical Societies Publishing

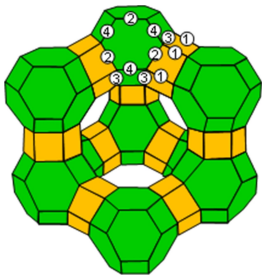

Scheme 1. FAU structure. The Si/Al atoms are the vertexes of the colored polyhedra, representative positions of oxygen atoms O(1)-O(4) are noted. Sodalite cages are depicted in green and D6R in yellow. In the center sits the supercage.

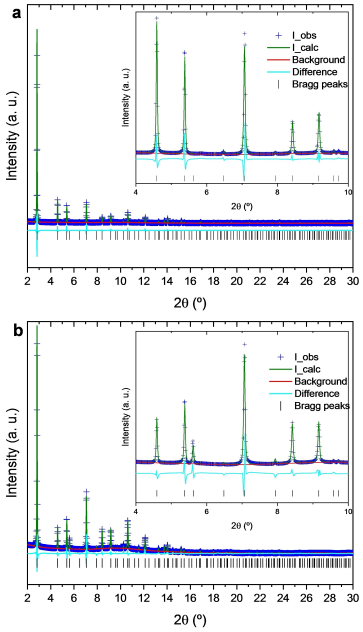

Figure 2. Observed (blue crosses), calculated (green curve) and weighted difference (turquoise) patterns (λ = 0.06919 nm) from Rietveld refinement using data from t = 0 (a) and 470 min (b). The insets present magnifications in the 4°-10° 2θ region.

positions *i* and *g* for carbon atoms within the supercages of the **FAU** structure was considered, corresponding to a crystallographic disordered carbon model. The fractional occupation of these positions was further revealed by the difference Fourier map established by Rietveld refinement of the pristine **FAU** model with the intensities of the experimental XRPD pattern after 470 min (**Figure S4**).

This allowed for evincing the evolution of the fractional occupation of the *i* and *g* positions and hence the number of total carbon atoms per unit cell (UC), (Figure 3a). These latter present a linear evolution as a function of the intensity of the 222 reflection, indicating that the number of carbon atoms directly correlates to the intensity evolution of this reflection (**Figure S5**). Both positions are gradually occupied during the experiments reaching a maximum of 0.97(30) and 0.68(16) for *i*

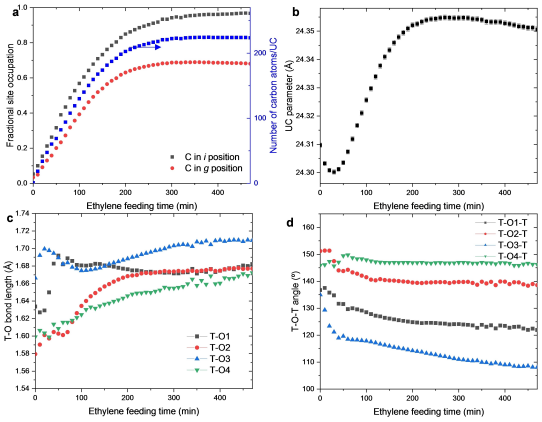

Figure 3. Evolution of the number of carbon atoms per UC and fractional occupation of the two carbon atom positions (a), of the unit cell parameter (b), of the T–O bond lengths (c) and of the T–O–T angles (d) as a function of ethylene feeding time. Estimated Standard Deviations (esd) are reported in table S1 and S2. R_{wp} and GOF are presented in Figure S6.

and *g*, respectively. This is pictured in Figure 4 for selected ethylene feeding times. A total number of 223 carbon atoms per UC is attained at the end of the experiment, which would correspond to a structural packing density (SPD) of 0.23 $g_C\ g_Z^{-1}$. This value is slightly below those experimentally reported (SPD = 0.30–0.36 $g_C\ g_Z^{-1}$, depending on synthesis conditions).[5] This difference can be explained by the presence of carbon atoms which might not contribute coherently to the observed diffraction signals. It is further to mention that SPD is invariably calculated from TGA data, hence overestimation of the value due to the presence of carbon on the external zeolite surface may not be excluded. The correlation of the 222 intensity with SPD and more strikingly with the residual zeolite micropore volume is foregrounded from *ex situ* experiments (supplemen-

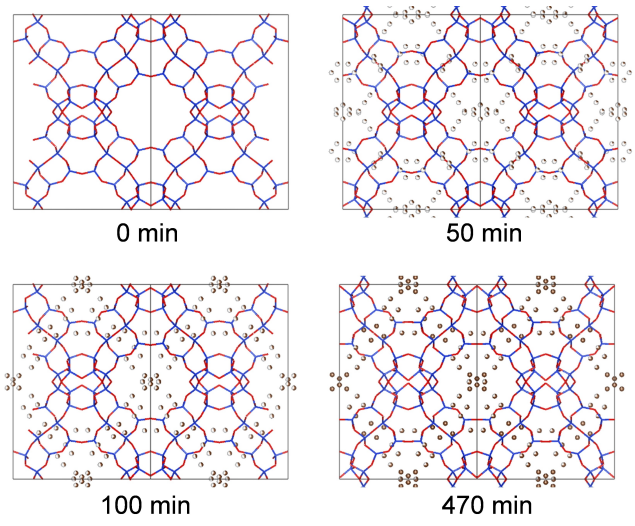

Figure 4. Refinement structural models for ethylene feeding times at t = 0, 50, 100 and 470 min, indicating atomic positions for carbon atoms with their corresponding fractional site occupation. Projection along the (110) plane. Color code: Si/Al: blue, O: red, C: brown. Drawings produced by VESTA.[29]

Research Article
doi.org/10.1002/cmtd.202400018
Chemistry Europe
European Chemical Societies Publishing

Table 1. Rietveld refinement parameters and statistics of fitting for t = 0 and 470 min.[a]

	Start of ethylene feeding (0 min)				End of ethylene feeding (470 min)			
UC parameter	24.3097(8) Å				24.3507(9) Å			
Atom positions	x	y	z	U_{iso} (Å^2)	x	y	z	U_{iso} (Å^2)
T (Si,Al)	−0.0530(4)	0.1229(5)	0.0373(4)	0.0339(28)	-0.0549(6)	0.1200(7)	0.0381(6)	0.109(5)
O1	0.00000	0.8937(7)	0.1063(7)	0.055(5)	0.00000	0.8930(12)	0.1070(12)	0.145(11)
O2	−0.0031(7)	−0.0031(7)	0.1388(10)	0.055(5)	-0.0016(10)	-0.0016(10)	0.1423(14)	0.145(11)
O3	0.0737(6)	0.0737(6)	-0.0184(9)	0.055(5)	0.0736(6)	0.0736(6)	-0.0068(12)	0.145(11)
O4	0.0741(9)	0.0741(9)	0.3177(10)	0.055(5)	0.0729(10)	0.0729(10)	0.3071(13)	0.145(11)
C1	−0.0530(4)	0.1229(5)	0.0373(4)	0.0339(28)	-0.0549(6)	0.1200(7)	0.0381(6)	0.109(5)
C2	0.516(21)	0.516(21)	0.465(20)	0.055(5)	0.5364(13)	0.5364(13)	0.4836(13)	0.145(11)
C1/C2 occupancies[b]	0.10(1)/0.01(8)				0.96(3)/0.68(2)			
$R_{wp\ (\%)}$	10.58				6.41			
$N_{var.}$	43				43			
$N_{obs.}$	2429				2429			
GOF	5.38				2.94			

[a] Estimated Standard Deviations are in parentheses. [b] Atomic site occupancies can be used to determine total number of carbon atoms considering the site multiplicity 96 and 192 for C1 and C2 respectively.

tary information). Slight variations of the UC parameter indicate that the developing carbon species within the zeolite voids impact the zeolite framework (Figure 3b, Table 1). This is further evidenced by the evolution of the T–O (T=Si, Al) bond lengths and T–O–T angles during the ethylene feeding experiment. The **FAU** structure comprises four crystallographic distinct O atoms: O(1), which bridge the two halves of the D6Rs; O(2), which connect the four-ring of D6R units and a six-ring of a the sodalite cages; O(3), which share four-rings from D6Rs and sodalite cages and O(4), which bridge three of the six edges of the hexagonal faces of the sodalite units (Scheme 1).

From the T–O bond length data (Figure 3c) it can be observed that the distances vary little during the ethylene feeding experiment, the mean distance increases from 1.616 to 1.680 Å (Table S1). Strongest modification of the bond distance was recorded for T–O(2) and T–O(4). Similarly, mean T–O–T angles decrease slightly during the experiment (Table S2). However significant modifications occur with individual T–O–T angles. The angles about O(2) and O(4) remain approximately constant, whilst a reduction for both T–O(1)-T and T–O(3)-T can be observed. The distortion of the T–O–T angles occurs on the 4-rings building up the D6Rs, which implies a stretching of the T–O distances in the 6-rings in the sodalite units. It is conspicuous that the degree of distortion accelerates after 100 min of the experiment, which suggest that the initially forming hydrocarbon species exert a weak impact on the zeolite framework.

It is important to mention that Havenga *et al.*[27] reported that amorphization of Y zeolite was triggered by the severe distortion of the D6Rs upon exposure to pressure. This observation was supported by the results of Colligan *et al.*,[28] who reported modifications in bond angles of the D6R units and reduction of the UC parameter by subjecting silicious **FAU** to external pressure. It is hence possible to hypothesize that the observed distortion of D6R units during ethylene feeding might result from local pressure exerted by the developing carbon skeleton on the zeolite structure.

It is interesting to note that by combining most of the previously described atomistic structures of ZTCs[30] with our pristine **FAU** model did not prove successful in reproducing the experimentally observed powder pattern of the carbon/zeolite hybrid. This is particularly true for the three distinct Nishihara models,[31,32] for which no enhancement of the 222 reflection could be observed (Figure 5). Intensity of the 222 reflection was observed for the Russel model[33] together with the appearance of reflections not present in the experimental pattern and not ascribable to the **FAU** structure. In 2016, Kim *et al.*[17] proposed a model, achieved from the electron-density map of a carbon/zeolite hybrid derived from X-ray single-crystal diffraction. This Kim model is based on the fractional occupation (0.10–0.22) of

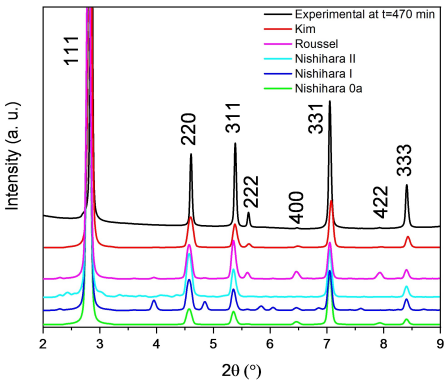

Figure 5. Comparison of the experimental XRPD pattern achieved at t = 470 min with simulated patterns by combining previously reported ZTC models[30] with the pristine FAU model. Intensities are normalized on the 111 reflection.

Research Article
doi.org/10.1002/cmtd.202400018
Chemistry Europe
European Chemical Societies Publishing

9 distinct sites. By comparing the simulated XRPD pattern using the Kim model with the experimental a stronger decrease in the intensity of the 220 and 331 reflections and a less pronounced increase of the 222 reflection can be observed. This suggests that the fractional occupation of the distinct sites proposed in the models is ill-defined, which might result from the non-inclusion of framework distortion during the assessment of electron density.

The refinement results in this study primarily provide insights into the evolution of occupancies at C1 and C2, offering limited direct information on the structural features of the emerging carbon species. However, by connecting the adjacent carbon atoms within these occupancies, the progression of carbon framework can be observed. At earlier stages (50 min), this method highlights the formation of smaller, individual polyaromatic hydrocarbons, consistent with our previous findings (Figure 6).[7] By the end of the synthesis (470 min), these units connect to form the condensed ZTC carbon skeleton. It is important to note that this structure should not be considered a definitive ZTC model due to the irregularity in site occupancy.

In order to achieve insights on the energetics of the ZTC formation, *in situ* XRPD experiments were carried out at different temperatures monitoring the intensity evolution of the 222 reflection (Figure 7). From the initial slope of the intensity profiles the rate constant could be determined, which allows calculating the apparent Arrhenius activation energy, amounting to 141 kJ mol^{-1}. This value is higher than the previously reported apparent activation energy for coke formation in USY zeolite (60–100 kJ mol^{-1}),[34] which suggests that coke formation and ZTC development might only partially be comparable processes. It is interesting to note that the obtained value falls in the range of the apparent activation energy reported for the nucleation and growth of graphene on copper (100–200 kJ mol^{-1}).[35]

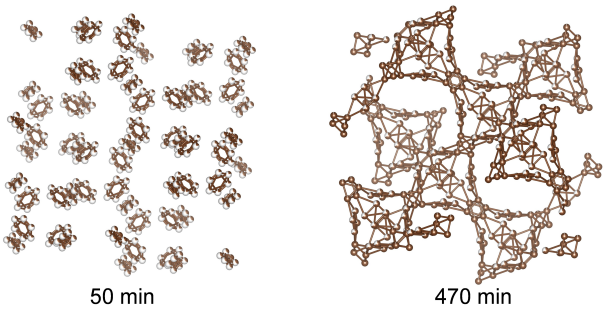

Figure 6. Conceptual model of carbon species at 50 and 470 min.

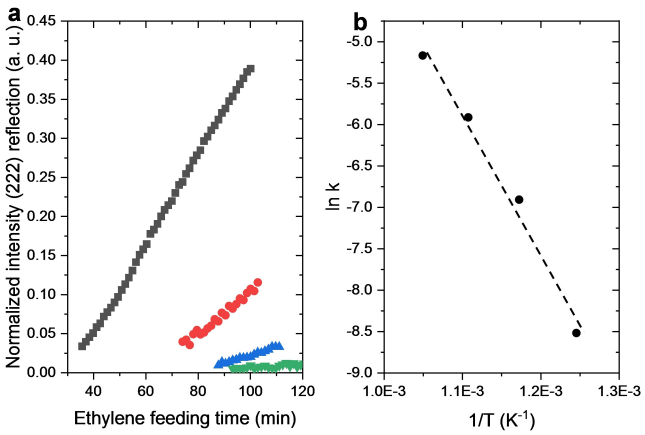

Figure 7. a) Intensity profile of the 222 reflection at different temperatures as a function of the ethylene feeding time and b) Arrhenius plot. Color code: 680 °C (black squares), 630 °C (red circles), 580 °C (blue triangles) and 520 °C (green triangles).

Conclusions

Rietveld refinement using synchrotron X-ray powder diffraction data on carbon/zeolite hybrid formation during ZTC synthesis revealed pattern modifications associated with progressive pore filling by carbon atoms. This process leads to a distortion of the zeolite framework, particularly in the six-rings of the D6R units, which becomes more pronounced with longer ethylene feeding times. This suggests that the developing ZTC skeleton exerts increasing internal pressure on the zeolite structure. Observing the evolution of the 222 reflection provides quantitative insights into the coherent contribution of developing carbon atoms to the diffraction pattern. This approach offers a robust method for evaluating carbon formation within the **FAU** zeolite structure, focusing exclusively on carbon within the zeolite voids, unlike SPD derived from TGA. This work could pave the way for the development of advanced structural models for ZTCs growing within **FAU** zeolite

Supporting Information

Details on experimental procedure, experimental setup for *in situ* XRPD synchrotron study, Le Bail refinement, Fourier Difference map, Statistics of fitting R_{wp} and GOF, Si–O distances, Si-O–Si angles, *ex situ* experiments, and Crystallographic Information Files can be found as Supporting Information. The authors have cited additional references within the Supporting Information.[35]

Acknowledgments

We acknowledge SOLEIL for provision of synchrotron radiation facilities (proposal 20201175). The authors acknowledge the European Union (ERDF) and Région Nouvelle Aquitaine and the French government program "Investissements d'Avenir" (EUR INTREE, reference ANR-18-EURE-0010). We thank Dr. Claudia Weidenthaler, Dr. Jean-Louis Paillaud and Dr. Taylan Örs for helpful discussions. We are further grateful to Bertrand Leroux, Michel Chauveau and Claude Veit for their assistance in the preparation and design of the experimental setup.

Conflict of Interests

The authors declare no conflict of interest.

Data Availability Statement

The data that support the findings of this study are available from the corresponding author upon reasonable request.

Keywords: Zeolite-Templated Carbon · XRD · Activation energy · Time resolved · Synchrotron · Coke

[1] G. Busca, *Microporous Mesoporous Mater.* **2017**, *254*, 3.
[2] K. Tanabe, W. F. Hölderich, *Appl. Catal. A* **1999**, *181*, 399.
[3] M. Guisnet, P. Magnoux, *Appl. Catal.* **1989**, *54*, 1.
[4] M. Guisnet, L. Costa, F. Ramôa Ribeiro, *J. Mol. Catal. A* **2009**, *305*, 69.
[5] T. Aumond, H. Vezin, I. Batonneau-Gener, S. Compère, Y. Pouilloux, A. Le Person, A. Moissette, A. Sachse, *Small* **2023**, *19*, 2300972.
[6] H. Nishihara, T. Kyotani, *Chem. Commun.* **2018**, *54*, 5648.
[7] T. Aumond, I. Batonneau-Gener, Y. Pouilloux, L. Pinard, D. Wisser, M. Moreau, H. Vezin, A. Moissette, A. Sachse, *Mater. Today Chem.* **2022**, *26*, 101053.
[8] T. Aumond, S. Compère, A. Sachse, *Microporous Mesoporous Mater.* **2024**, *367*, 112967.
[9] Y. Liu, J. Wang, M. A. Seragelding, T. Wang, W.-P. Pan, *Microporous Mesoporous Mater.* **2021**, *324*, 111311.
[10] H. Nishihara, K. Imai, H. Itoi, K. Nomura, K. Takai, T. Kyotani, *Tanso* **2017**, *280*, 169.
[11] L. Aouali, J. Jeanjean, A. Dereigne, P. Tougne, D. Delafosse, *Zeolites* **1988**, *8*, 517.
[12] D. M. Bibby, N. B. Milestone, J. E. Patterson, L. P. Aldridge, *J. Catal.* **1986**, *97*, 493.
[13] F. Bauer, V. Kanazirev, L. Vlaev, R. Hanisch, W. Weiss, *Chem. Tech.* **1989**, *41*, 297.
[14] A. G. Alvarez, H. Viturro, R. D. Bonetto, *Mater. Chem. Phys.* **1992**, *32*, 135.
[15] M. A. Uguina, D. P. Serrano, R. Van Grieken, S. Vènes, *App. Catal. A* **1993**, *99*, 97.
[16] M. Rozwadowski, J. Włoch, K. Erdmann, J. Kornatowski, *Collect. Czech. Chem. Commun.* **1992**, *57*, 959.
[17] K. Kim, T. Lee, Y. Kwon, Y. Seo, J. Song, J. Ki Park, H. Lee, J. Young Park, H. Ihee, S. June Cho, R. Ryoo, *Nature* **2016**, *535*, 131.
[18] A. Coati, L. M. G. Chavas, P. Fontaine, N. Foos, B. Guimaraes, P. Gourhant, P. Legrand, J.-P. Itie, P. Fertey, W. Shepard, T. Isabet, S. Sirigu, P.-L. Solari, D. Thiaudiere, A. Thompson, *Eur. Phys. J. Plus* **2017**, *132*, 174.
[19] Y. Sakamoto, N. Togashi, O. Terasaki, T. Ohsuna, Y. Okamoto, K. Hiraga, *Mater. Sci. Eng. A* **1996**, *217–218*, 147.
[20] J. Smith, J. Bennett, E. Flanigen, *Nature* **1967**, *215*, 241.
[21] X. Du, H. Zhang, X. Li, Z. Tan, H. Liu, X. Gao, *Chin. J. Catal.* **2013**, *34*, 1599.
[22] N.-N. Wang, Y. Wang, H.-F. Cheng, M.-E. Fu, Z. Tao, W.-Z. Wu, *J. Porous Mater.* **2013**, *20*, 1371.
[23] A. Dosen, B. A. Marinkovic, *Bull. Mater. Sci.* **2019**, *42*, 86.
[24] B. F. Mentzen, *C. R. Chim.* **2005**, *8*, 353.
[25] A. N. Fitch, H. Jobic, A. Renouprez, J. Phys, *Chem.* **1986**, *90*, 1311.
[26] T. Aumond, A. Le Person, I. Batonneau-Gener, H. Vezin, A. Sachse, A. Moissette, J. Phys, *Chem.* C **2023**, *127*, 3486–3496.
[27] E. A. Havenga, Y. Huang, R. A. Secco, *Mater. Res. Bull.* **2003**, *38*, 381.
[28] M. Colligan, P. M. Forster, A. K. Cheetham, Y. Lee, T. Vogt, J. A. Hriljac, *J. Am. Chem. Soc.* **2004**, *126*, 12015.
[29] K. Momma, F. Izumi, *J. Appl. Crystallogr.* **2011**, *44*, 1272.
[30] E. E. Taylor, K. Garman, N. P. Stadie, *Chem. Mater.* **2020**, *32*, 2742.
[31] H. Nishihara, Q.-H. Yang, P.-X. Hou, M. Unno, S. Yamauchi, R. Saito, J. I. Paredes, A. Martínez-Alonso, J. M. D. Tascón, Y. Sato, M. Terauchi, T. Kyotani, *Carbon* **2009**, *47*, 1220.
[32] H. Nishihara, H. Fujimoto, H. Itoi, K. Nomura, H. Tanaka, M. T. Miyahara, P. A. Bonnaud, R. Miura, A. Suzuki, N. Miyamoto, N. Hatakeyama, A. Miyamoto, K. Ikeda, T. Otomo, T. Kyotani, *Carbon* **2018**, *129*, 854.
[33] T. Roussel, A. Didion, R. J.-M. Pellenq, R. Gadiou, C. Bichara, C. Vix-Guterl, J. Phys, *Chem. Can.* **2007**, *111*, 15863.
[34] A. A. Brillis, G. Manos, *Ind. Eng. Chem. Res.* **2003**, *42*, 2292.
[35] H. Kim, C. Mattevi, M. Reyes Calco, J. C. Oberg, L. Artiglia, S. Agnoli, C. F. Hirjibehedin, M. Chhowalla, E. Saiz, *ACS Nano* **2012**, *6*, 3614.

Manuscript received: June 26, 2024
Version of record online: ■■, ■■